Atmos. Chem. Phys., 14, 9925–9939, 2014
www.atmos-chem-phys.net/14/9925/2014/
doi:10.5194/acp-14-9925-2014

Atmospheric Chemistry and Physics
Open Access

Aviation 2006 NO_x-induced effects on atmospheric ozone and HO_x in Community Earth System Model (CESM)

A. Khodayari[1], S. Tilmes[3], S. C. Olsen[2], D. B. Phoenix[2], D. J. Wuebbles[2], J.-F. Lamarque[3], and C.-C. Chen[3]

[1]Department of Civil and Environmental Engineering, University of Illinois at Urbana-Champaign, Urbana, IL 61801, USA
[2]Department of Atmospheric Sciences, University of Illinois at Urbana-Champaign, Urbana, IL 61801, USA
[3]National Center for Atmospheric Research, Boulder, CO, USA

Correspondence to: A. Khodayari (akhoday2@illinois.edu)

Received: 14 January 2014 – Published in Atmos. Chem. Phys. Discuss.: 7 March 2014
Revised: 24 July 2014 – Accepted: 24 July 2014 – Published: 19 September 2014

Abstract. The interaction between atmospheric chemistry and ozone (O_3) in the upper troposphere–lower stratosphere (UTLS) presents a major uncertainty in understanding the effects of aviation on climate. In this study, two configurations of the atmospheric model from the Community Earth System Model (CESM), Community Atmosphere Model with Chemistry, Version 4 (CAM4) and Version 5 (CAM5), are used to evaluate the effects of aircraft nitrogen oxide ($NO_x = NO + NO_2$) emissions on ozone and the background chemistry in the UTLS. CAM4 and CAM5 simulations were both performed with extensive tropospheric and stratospheric chemistry including 133 species and 330 photochemical reactions. CAM5 includes direct and indirect aerosol effects on clouds using a modal aerosol module (MAM), whereby CAM4 uses a bulk aerosol module, which can only simulate the direct effect. To examine the accuracy of the aviation NO_x-induced ozone distribution in the two models, results from the CAM5 and CAM4 simulations are compared to ozonesonde data. Aviation NO_x emissions for 2006 were obtained from the AEDT (Aviation Environmental Design Tool) global commercial aircraft emissions inventory. Differences between simulated O_3 concentrations and ozonesonde measurements averaged at representative levels in the troposphere and different regions are 13 % in CAM5 and 18 % in CAM4. Results show a localized increase in aviation-induced O_3 concentrations at aviation cruise altitudes that stretches from 40° N to the North Pole. The results indicate a greater and more disperse production of aviation NO_x-induced ozone in CAM5, with the annual tropospheric mean O_3 perturbation of 1.2 ppb (2.4 %) for CAM5 and 1.0 ppb (1.9 %) for CAM4. The annual mean O_3 perturbation peaks at about 8.2 ppb (6.4 %) and 8.8 ppb (5.2 %) in CAM5 and CAM4, respectively. Aviation emissions also result in increased hydroxyl radical (OH) concentrations and methane (CH_4) loss rates, reducing the tropospheric methane lifetime in CAM5 and CAM4 by 1.69 and 1.40 %, respectively. Aviation NO_x emissions are associated with an instantaneous change in global mean short-term O_3 radiative forcing (RF) of 40.3 and 36.5 mWm^{-2} in CAM5 and CAM4, respectively.

1 Introduction

The aviation industry has grown rapidly since its nascence, at a rate of 9 % per year for passenger traffic between 1960 and 2000 (IPCC, 1999) and is one of the fastest growing transportation sectors (IPCC, 2007). Despite several international economic and other setbacks over the last few decades, including large price increases for fuel, and a global recession, the aviation industry continues to experience growth. The 2013 FAA forecast calls for an annual average increase of 2.2 % per year in US passenger carrier growth over the next twenty years. The growth is predicted to be slightly greater for the first five years under the assumption of a faster US economic growth rate (FAA, 2013). As such, it is important to assess the potential impacts that aviation will have on future climate.

Aviation affects climate in various ways. The main concerns to climate result from the emissions of carbon dioxide (CO_2) and nitrogen oxides ($NO_x = NO + NO_2$), which influence the gas-phase and aerosol chemistry. Other aviation-induced impacts result from the emissions of H_2O, and the

emission of sulfate and soot particles, which influence the formation of contrail-cirrus clouds and change the cloudiness by acting as cloud condensation nuclei (e.g., Gettelman et. al., 2012). The resulting effects of these emissions modify the chemical properties of the upper troposphere–lower stratosphere and the cloud microphysics that affect the Earth's climate system radiative forcing. For the majority of these effects, the radiative forcing is positive; however, for sulfate particles – which reflect incoming shortwave radiation, and for the increases in OH concentrations – which reduce the CH_4 concentrations, the radiative forcing is negative (Lee et al., 2009). The indirect effect of sulfate aerosols may, on the other hand, result in a negative radiative forcing via liquid clouds which dominates the warming caused from contrails and black carbon (BC) emissions (Gettelman et al., 2013). This study will focus on the aviation NO_x-induced effects, and particularly the NO_x-induced effect on atmospheric ozone (O_3).

There have been many previous studies that examined the effect of aviation NO_x emissions on NO_x-induced O_3 (e.g., Derwent et al., 1999; Fuglestvedt et al., 1999; Wild et al., 2001; Derwent et al., 2001; Stevenson et al., 2004; Köhler et al., 2008; Hoor et al., 2009; Koffi et al., 2010; Hodnebrog et al., 2011). The aviation NO_x-induced changes in O_3 calculated in these studies varies between 0.46 and 0.90 Dobson units of ozone per TgN per year ($DU(O_3)\,[TgN\,yr^{-1}]^{-1}$). Other recent studies have examined the factors that control the production of NO_x-induced O_3. Stevenson and Derwent (2009) found that the O_3 and CH_4 response to NO_x emissions varies regionally, and are most sensitive in regions with low-background NO_x concentrations. Several studies analyzed the impact of the location and time of the emissions (Derwent et al., 2001; Stevenson et al., 2004). Derwent et al. (2001) analyzed the changes in methane and tropospheric ozone after emitting pulses of NO_x at the surface and upper troposphere in both the Northern and Southern hemispheres and found that while the changes in methane radiative forcing were dominated by methane emissions, changes in tropospheric ozone radiative forcing were dominated by changes in ozone precursor gases, notably NO_x emissions. Stevenson et al. (2004) looked at the effects of an extra pulse of aviation-induced NO_x at four months representing the seasonal cycle. Their results showed a seasonal dependence in the O_3 radiative forcing with a long-term net radiative forcing of approximately zero. Wild et al. (2012) examined the impact of solar-flux variations, while Shine et al. (2005) and Berntsen et al. (2005) investigated the effects of atmospheric mixing. However, as reported in Holmes et al. (2011), model-based estimates of aviation NO_x-induced changes in O_3 vary by up to 100 %, largely because of differences between models in the ratios of $NO : NO_2$ and $OH : HO_2$, background NO_x levels, location and time of emissions, the amount of sunlight, and in atmospheric mixing (Holmes et al., 2011). Recent studies by Olsen et al. (2013) and Brasseur et al. (2014) found considerable differences between a set of climate–chemistry models (CCMs) and chemistry transport models (CTMs) in comparisons of the background atmosphere and aviation NO_x-induced changes in ozone.

In this study, we examine the effect of aviation NO_x emissions on the atmospheric concentration of O_3 and hydrogen oxide radicals ($HO_x = OH + HO_2$) and the reduction of CH_4 lifetime using the latest versions of the atmospheric components of the Community Earth System Model (CESM) model, namely the Community Atmosphere Model with Chemistry, Version 4 (CAM4) and Version 5 (CAM5). We further calculate the radiative forcing associated with the changes in O_3 concentration using the University of Illinois Radiative Transfer Model (UIUC RTM). While the calculated effects in CAM4 and CAM5 provide a new reference for the aviation NO_x-induced effects in comprehensive climate–chemistry models, they also provide a measure for the effects of different oxidative capacity in the models, due to differences in description of the physical processes in the model, and especially due to the different treatment of aerosol processes (see model description).

This paper is organized as follows. The following section provides model description. Section 3 discusses the emissions and simulation setup. Section 4 presents the results and Sect. 5 provides the concluding material.

2 Model description

CAM4 and CAM5 (Community Atmosphere Model versions 4 and 5) are the atmospheric component models for the Community Earth System Model (CESM) (http://www.cesm.ucar.edu/). The details of the physics parameterizations in the CAM4 and CAM5 models have been discussed extensively in other studies before (e.g., Neale et al., 2011; Gent et al., 2011; Lamarque et al., 2012). Briefly, CAM5 has been substantially modified in the representation of physical processes compared to CAM4, including a new shallow convection scheme, updated planetary boundary layer (PBL) schemes, revised cloud macrophysics scheme, and updated radiation scheme (Medeiros et al., 2012). These updates improve the representation of cloud properties and permit assessing the indirect effect of aerosols on clouds, which is not included in CAM4.

Cloud microphysical processes in CAM5 are represented by a prognostic, two-moment formulation for cloud droplets and cloud ice. Mass and number concentrations of cloud droplets and cloud ice follow the Morrison and Gettelman (2008) parameterization. The gamma function is employed to determine liquid and ice particle sizes (Gettelman et al., 2008). The evolution of liquid and ice particles in time is affected by grid-scale advection, convective detrainment, and turbulent diffusion. Activation of cloud droplets is a function of aerosol size distribution, aerosol chemistry, temperature, and vertical velocity (Neale et al., 2011). The cloud macrophysics scheme imposes full consistency between cloud

fraction and cloud condensate. Liquid cloud fraction is based on a triangular distribution of total relative humidity. Ice cloud fraction is based on Gettelman et al. (2010) that allows supersaturation via a modified relative humidity over ice and the inclusion of the ice condensate amount. The aerosol–cloud scheme simulates full aerosol–cloud interactions such as cloud droplet activation by aerosols, precipitation processes due to particle size dependence, and explicit radiative interaction of cloud particles (Liu et al., 2012).

Further, CAM5 was successfully coupled to the full chemical mechanism and released in CESM 1_2_0 and versions thereafter (as discussed in detail in Tilmes et al., 2014). Since the coupling of aerosols and chemistry in CAM5 has not been released at the time model runs were performed, a development version of close to CESM1_2_0 release version (cesm1_2_beta08_chem) was used for CAM5 simulations, which includes this coupling. The CESM1_0_3 released version was used for CAM4 simulations. Both models use the same photolysis scheme as described in Lamarque et al. (2012) and use the same gas-phase chemical mechanisms including tropospheric and stratospheric chemistry with about 133 species and 330 photochemical reactions (Lamarque et al., 2012). A complete list of species and reactions can be found in Lamarque et al. (2012). While the two models use the same gas-phase chemistry, there are differences in aerosol properties, due to the different aerosol treatment in CAM4 and CAM5. CAM4 uses a bulk aerosol module with one lognormal distribution for all aerosols (Lamarque et al., 2012), while CAM5 uses the modal aerosol module (MAM) (Liu et al., 2012). MAM was developed with two versions, one with seven lognormal modes (MAM7) and one with three lognormal modes (MAM3) (Liu et al., 2012). Here, we use the more complete version with seven lognormal modes. MAM7 represents Aitken, accumulation, primary carbon, fine dust and sea salt, and course dust and sea salt modes. Within each mode, the mass mixing ratios of the respected aerosols and their number mixing ratios are calculated (Liu et al., 2012). MAM simulates both internal and external mixing of aerosols, chemical and optical properties of aerosols, and various complicated aerosols processes (Liu et al., 2012).

The UIUC RTM was used offline to calculate the forcing associated with aviation NO_x-induced short-term O_3. Earlier versions of the UIUC RTM have been used in previous research (e.g., Jain et al., 2000; Naik et al., 2000; Youn et al., 2009; Patten et al., 2011). The UIUC RTM calculates the flux of solar and terrestrial radiation across the tropopause. The solar model includes 18 spectral bins from 0.2 to 0.5 microns and includes absorption by H_2O, O_3, O_2, CO_2, clouds, and the surface. Scattering processes by clouds, gas-phase molecules, and the surface are included as well. The terrestrial radiation calculation uses a narrow band model of absorptivity and emissivity that covers wave numbers from 0 to 3000 cm^{-1} at a resolution of 10 cm^{-1} for H_2O, CFC-11, and CFC-12, and of 5 cm^{-1} for all other gases. The infrared absorption parameters for gases are obtained from the HITRAN 2004 database (Rothman et al., 2005). Surface albedo and emissivity are based on observations, while clouds are based on the International Satellite Cloud Climatology Project. The use of the same cloud fields for both CAM4 and CAM5 simulations in the offline radiative forcing calculations ensures that the differences in the calculated change in radiative forcing are due to the differences in chemistry and not due to the differences in cloud fields. A previous study by Conley et al. (2013) shows that using different cloud fields in an offline radiative transfer model makes very little to no difference in the calculated change of radiative forcing for radiative active species.

3 Aviation NO_x emissions and simulation setup

Both models were run at a horizontal resolution of 1.9° latitude × 2.5° longitude and were configured with 56 vertical levels covering from the surface up to ∼ 2 hPa with near tropopause resolution of about 1.3 km. To reduce year-to-year climate variability in the model simulations and to help detect the aviation NO_x signal, specified dynamics ("offline" mode) simulations were performed. In these simulations, changes in the chemical constituents do not affect the dynamics. The models used the GEOS DAS v5.1 meteorology for the year 2005 (Rienecker et al., 2008) which was the closest available assimilated meteorology data to the year of interest (2006). The aviation emissions for 2006 are from the AEDT aviation emissions analyses (Wilkerson et al., 2010; Olsen et al., 2013). The background emissions of non-aviation short-lived species (e.g., NO_x, volatile organic compounds, VOCs) were obtained from the IPCC RCP4.5 scenario for year 2005 (van Vuuren et al., 2011) and both models were run with the same total lighting NO_x values. The monthly surface concentrations of longer-lived species, e.g., CO_2, CH_4, chlorofluorocarbons (CFCs), and nitrous oxide (N_2O), were specified as boundary conditions based on the IPCC RCP4.5 scenario. To analyze the effect of aviation NO_x emissions on the background atmosphere, two simulations are performed in each model. One simulation considers all NO_x emissions including aviation NO_x, and the other simulation has all NO_x emissions but no aviation NO_x (control run). The difference between these two simulations corresponds to the changes induced by aviation NO_x. The simulations were run for 7 years, cycling through the 2005 meteorology, to reach steady state with data from the seventh year used in this analysis.

Since both models were run with same emissions, same total lighting NO_x values, and with identical meteorological fields with 100 % nudging, the differences in the description of aerosols very likely have the largest impact on the chemistry of aviation NO_x-induced effects. In particular, differences in the aerosol burden, but especially in the surface area density, that are caused by differences in the aerosol

size distribution (effective radius) and mass, have an influence on the heterogeneous chemistry and therefore influence the oxidative capacity of the atmosphere and therefore the chemical composition, as further discussed in Sect. 4.4. It is noted that the differences in clouds caused by the differences in aerosol–cloud microphysical interactions between the two models may also contribute to differences in the chemistry of aviation NO_x-induced effects to some degree as it affects the radiation budget and therefore, the photolysis. The impact of differences in dynamics is expected to be small, since in both models the horizontal winds, surface fluxes, and temperatures were prescribed with GEOS meteorological analysis fields.

4 Results and discussions

4.1 Chemistry diagnosis

Previous intercomparisons of multiple climate–chemistry models indicated that CAM reasonably simulates the effects of aviation NO_x-induced emissions on distribution of tropospheric O_3 and NO_x (Weber, 2011; Olsen et al., 2014). However, due to the radiative importance of ozone in troposphere and stratosphere and in relation to differences in aerosols treatment between the two model configurations used in this study, simulated ozone in the control runs at representative altitudes is evaluated using an ozonesonde climatology (Tilmes et al., 2012). This climatology includes observations for the years 1995–2011 and covers averaged ozone profiles for 41 different ozonesonde stations that are grouped into 12 regions. For our comparisons, we evaluate ozone at four pressure levels covering the troposphere–lower stratosphere (50, 250, 500, and 900 hPa) over the 12 areas, which are grouped into three larger regions (tropics, mid-Latitudes, and high latitudes), as shown in Fig. 1. Model results are interpolated horizontally to all the stations within each region, and averaged over each region. The comparison between model and observations is illustrated in Taylor-like diagrams for each of the corresponding pressure levels and regions. A slightly different version of CAM4 including chemistry has been previously tested against ozone observations as well as the observations of other major atmospheric compounds (e.g., Lamarque et al., 2012).

The two model versions are in good agreement at 50 hPa and agree within 10 % with the observed values for the mid- and high latitudes, which is the range of the uncertainly of the observations, besides for Japan (deviations to observations are around 15 %) and for the Southern Hemisphere (SH) Polar region for CAM4. The seasonal cycle is well reproduced. The models overestimate the observed ozone concentration in the tropics by 25 to 50 %, with a poor description of the seasonal cycle, especially for CAM5.

At 250 hPa, both models reproduce high-latitude ozone observations within 25 % and show a reasonable agreement with the seasonal cycle. In the tropics and mid-latitudes, the model largely overestimates ozone, especially for Japan and the SH and most of the tropical stations. The overestimate of ozone in the mid-latitudes and tropics in CAM4 was also found in Lamarque et al. (2012), who noted that this result is an indication of a model estimated tropopause that is lower than observed and possibly too much transport of ozone into the troposphere.

Of the four pressure levels studied, the models most accurately simulate ozone at the 500 hPa level. The absolute difference in generated ozone is within 11.7 % for both models, which is within the variability of the observations. CAM4 slightly overestimates ozone at all but one location. Overall, CAM5 appears to perform better than CAM4 due to a lower percent difference in ozone (6.0 % in CAM5 compared to 11.7 % in CAM4). The seasonal cycle is simulated reasonably well for both models, with a correlation coefficient of 0.80 for CAM5 and 0.82 for CAM4.

On average, both models perform well in the boundary layer (900 hPa), although there are several outliers. Both models overestimate the ozone concentration in the Western Europe and Canada regions. On the other hand, both models underestimate ozone in the SH mid-Latitude and SH Polar regions. At all other locations, ozone agrees well with observations. The relative bias is lower in CAM5 (10.0 % compared to 15.7 % in CAM4), indicating a better representation of ozone by CAM5. Additionally, with the exception of the equatorial Americas region in CAM4 and the Japan region for both models, the seasonal correlation is excellent (0.81 in both CAM5 and CAM4).

Overall, both models simulate ozone more accurately in the troposphere than in the UTLS and stratosphere and overestimate ozone in the tropical transition layer. The simulated seasonal cycle in CAM4 is slightly better than in CAM5 in comparison to observations.

Comparisons of O_3, NO_x, HNO_3, PAN, as well as CO to aircraft observations between 2 and 7 km (Emmons et al., 2010; Tilmes et al., 2014), where the majority of the observations were taken is also shown in Fig. 2, both the control and perturbed simulations.

In comparison to aircraft data, ozone is slightly overestimated in the tropics, especially for the perturbed simulations, in agreement with ozonesonde observations, while there is reasonable agreement in mid- and high latitudes. Both model versions simulate the regional differences in NO_x in comparison to available aircraft observations reasonably well, but NO_x is slightly underestimated by all model simulations is summer in Northern Hemisphere (NH) mid-latitudes. Both model versions overestimate PAN and HNO_3 in tropics and mid-latitudes and high latitude in spring. Model differences between CAM4 and CAM5 are within the variability of the observations. CO is underestimated in both model versions, with much larger deviations from the observations for CAM5 than CAM4. This points to a significant overestimation of OH in CAM5, as also indicated by the smaller methane

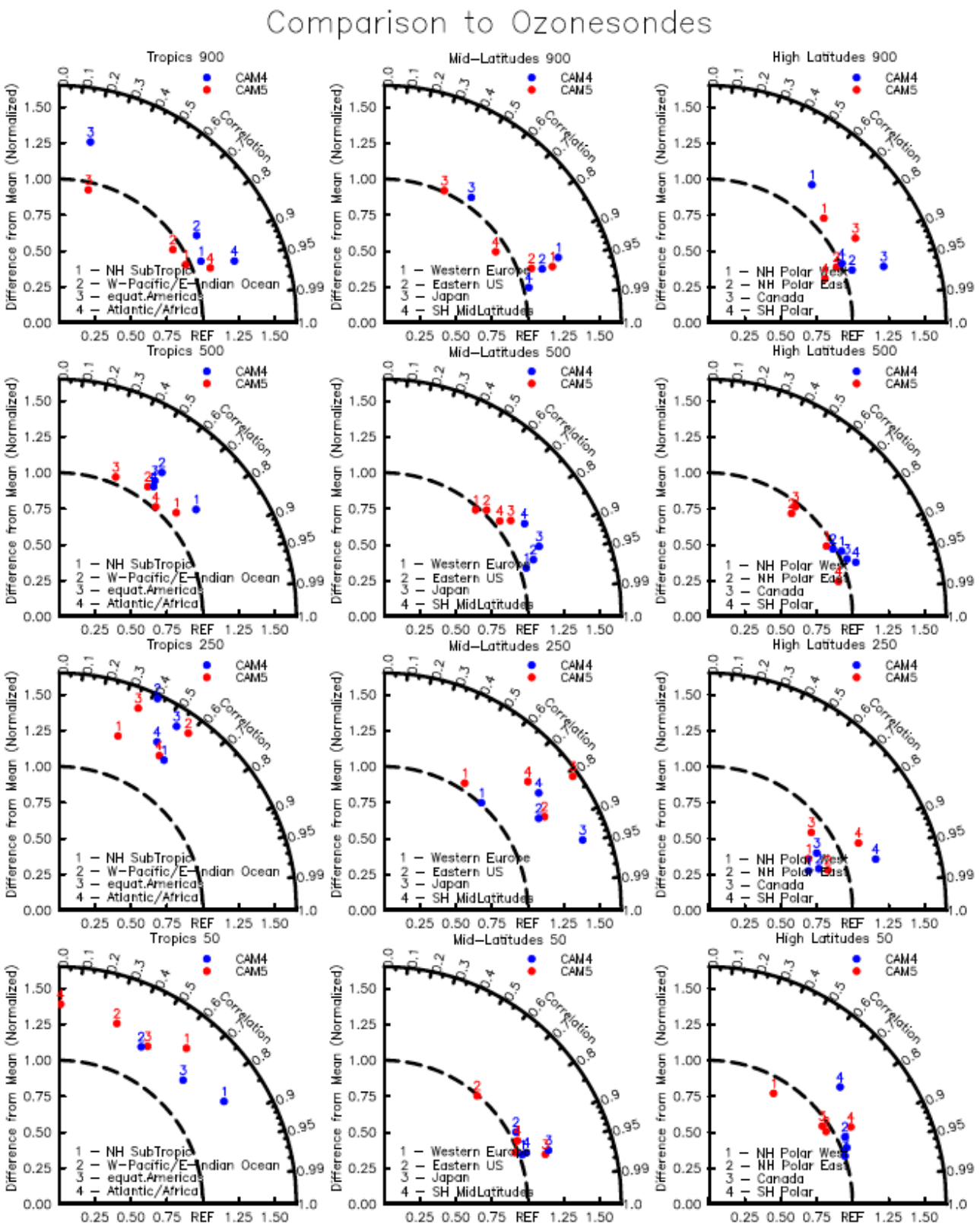

Figure 1. Taylor diagram of modeled background ozone from the control runs against ozonesonde climatology for four pressure levels and three latitudinal regions. REF along the abscissa denotes the observations while the radial distance describes the normalized bias. The correlation for the seasonal cycle is described along the angle.

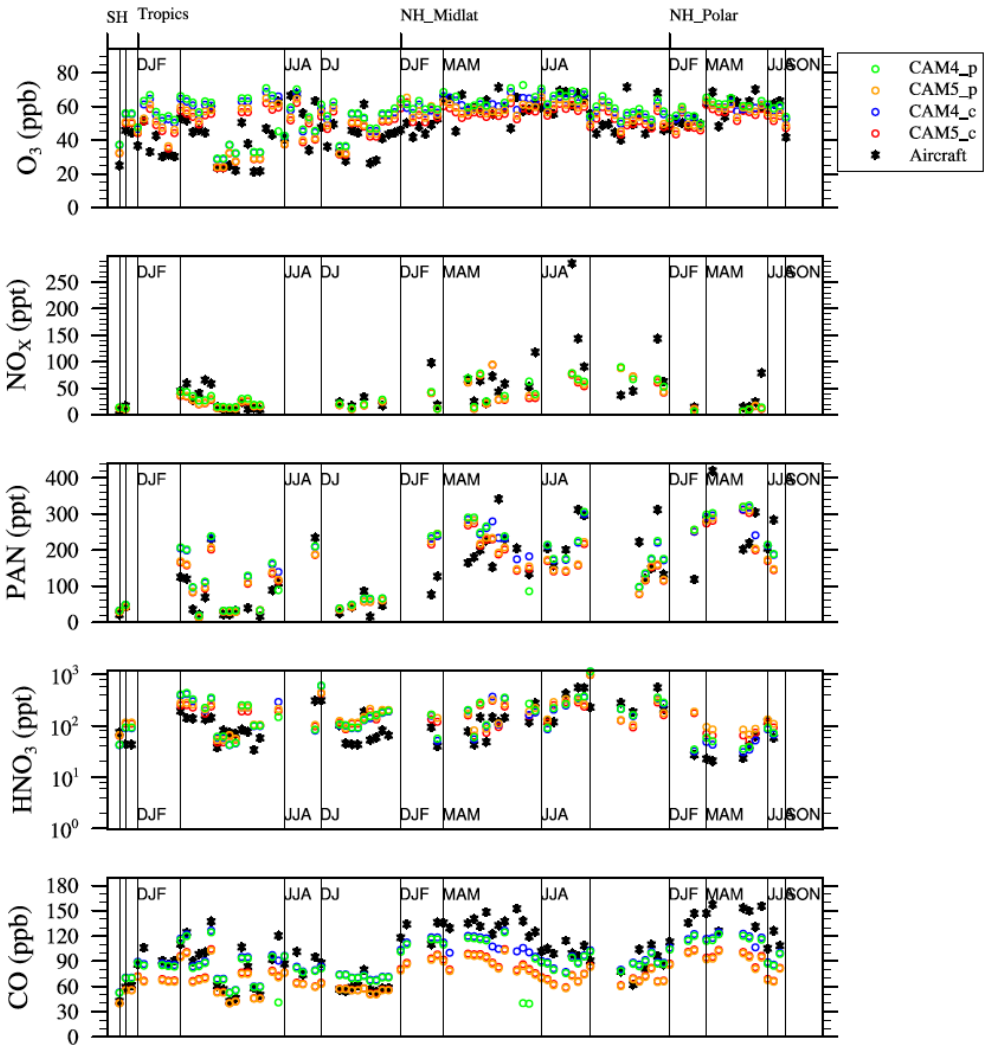

Figure 2. Comparison between aircraft observations over different regions and seasons and different model simulation, averaged between 2 and 7 km, for ozone, NO_x, PAN, HNO_3, and CO, based on an updated version of the aircraft climatology by Emmons et al. (2000), as described in detail in Tilmes et al. (2014). *_p and *_c refer to the perturbed and control simulations, respectively.

lifetime in CAM5 compared to CAM4. The increase in NO_x due to aircraft emissions does not affect NO_x, NO_y, and CO very much in the altitude considered. However, ozone is slightly increased in the perturbed case for both CAM4 and CAM5.

4.2 Spatial distribution of NO_x emissions

The AEDT NO_x emission data used as the input to the model runs had an hourly temporal resolution. The spatial distribution of aviation NO_x emissions for 2006 is shown in Fig. 3 which amounts to 2.7 Tg (NO_2) yr^{-1}. As in Fig. 3, the largest intensity of NO_x emissions is in the eastern United States, eastern Asia, and Europe. The local maximum in the eastern US contributes approximately 0.0136 Tg to the global emissions of NO_2, while the local maximum in Europe contributes 0.0154 Tg. Additionally, the peak value in Asia contributes 0.0123 Tg to the global total. These values represent the maximum emissions from a single grid cell. The main source of NO_x emissions occur between 30° and 60° N latitude.

Figure 4 shows the seasonal distribution of aviation NO_x emissions from 2006. As shown in Fig. 4, aviation NO_x emissions have a different seasonal distribution with the highest amount of emissions released in the summer, due to increased air traffic in those months.

4.3 Ozone production and loss

Figure 5 shows the aviation NO_x-induced annual vertical profile of short-term O_3 production and loss as calculated by CAM5 (red) and CAM4 (blue). Both models show the maximum rate of ozone production peaking in the upper

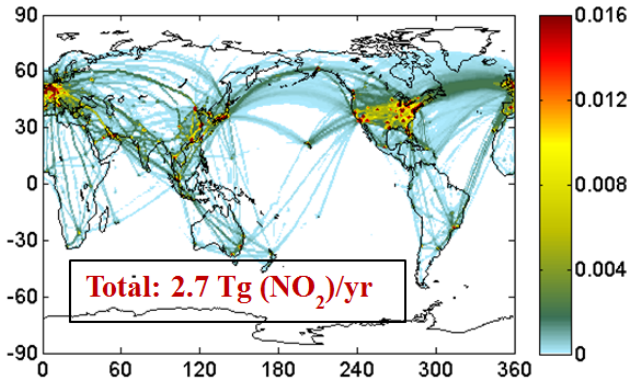

Figure 3. Spatial distribution of vertically integrated aviation NO_x emissions for 2006.

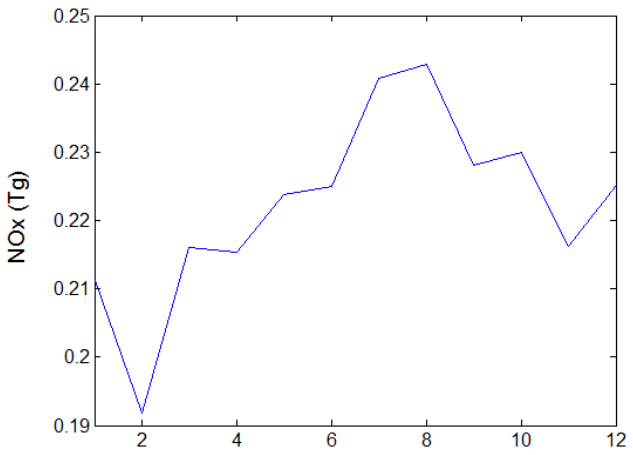

Figure 4. Seasonal distribution of global aviation NO_x emissions for 2006.

troposphere–lower stratosphere (UTLS) region where the greatest amount of aircraft-induced NO_x emissions occur.

As we analyze the results from the model runs, we use the following chemical reactions for ozone production in the troposphere (Sillman, 2012).

P1 $\mathrm{VOC} + \mathrm{OH} \xrightarrow{\mathrm{O_2}} \mathrm{RO_2} + \mathrm{H_2O}$

P2 $\mathrm{CO} + \mathrm{OH} \xrightarrow{\mathrm{O_2}} \mathrm{HO_2} + \mathrm{CO_2}$

P3 $\mathrm{RO_2} + \mathrm{NO} \xrightarrow{\mathrm{O_2}} \text{secondary VOC} + \mathrm{HO_2} + \mathrm{NO_2}$

P4 $\mathrm{HO_2} + \mathrm{NO} \rightarrow \mathrm{OH} + \mathrm{NO_2}$

P5 $\mathrm{NO_2} + h\nu \rightarrow \mathrm{NO} + \mathrm{O}$

P6 $\mathrm{O} + \mathrm{O_2} + \mathrm{M} \rightarrow \mathrm{O_3} + \mathrm{M}$

Ozone destruction in the troposphere, on the other hand, is given by the following reactions (Sillman, 2012).

L1 $\mathrm{NO} + \mathrm{O_3} \rightarrow \mathrm{NO_2} + \mathrm{O_2}$

L2 $\mathrm{O_3} + \mathrm{h}\nu \xrightarrow{\mathrm{H_2O}} 2\mathrm{OH} + \mathrm{O_2}$

L3 $\mathrm{HCHO} + \mathrm{h}\nu \xrightarrow{2\mathrm{O_2}} 2\mathrm{HO_2} + \mathrm{CO}$

L4 $\mathrm{HO_2} + \mathrm{HO_2} \rightarrow \mathrm{H_2O_2} + \mathrm{O_2}$

L5 $\mathrm{RO_2} + \mathrm{HO_2} \rightarrow \mathrm{ROOH} + \mathrm{O_2}$

L6 $\mathrm{OH} + \mathrm{NO_2} \rightarrow \mathrm{HNO_3}$

The impact of aviation-induced NO_x on ozone results in a net increase in the rate of ozone production with a maximum around 250 hPa, and a net decrease in the rate of ozone production ozone below 450 hPa. Within the UTLS region, the rate of ozone loss decreases due to the increase in HO_2 (Fig. 9, as discussed below) reacting with NO (as in Reaction P4). This process creates NO_2 which further increases O_3 production (by Reactions P5 and P6). Part of the excess ozone that is created in the UTLS region is transported to lower altitudes. As shown in Fig. 5, the rate of ozone loss peaks around 500 hPa. As described by Reaction (L2), at this altitude, excess ozone transported from the UTLS region in the presence of water vapor reacts to form HO_x, increasing ozone loss. Additional reductions in the net O_3 production are caused by the increased reaction of HO_x with NO_x near the surface, resulting in the conversion of NO_x to HNO_3 (Reaction L6).

While the patterns of the changes in the simulated ozone production and loss agree well between the models and with previous studies (Köhler et al., 2008), there are differences between CAM4 and CAM5 in the magnitudes. Compared to CAM4, overall ozone production and loss are larger in CAM5, due to the differences in OH between the models. The net rate of ozone production in CAM5 is higher at cruise altitudes and slightly lower at lower altitudes. The maximum net production of ozone is 1.1×10^{20} molecules $\mathrm{s^{-1}}$ $\mathrm{Pa^{-1}}$ in CAM5 and 1.0×10^{20} molecules $\mathrm{s^{-1}}$ $\mathrm{Pa^{-1}}$ in CAM4. CAM4 estimates a maximum rate of production at 1.2×10^{20} molecules $\mathrm{s^{-1}}$ $\mathrm{Pa^{-1}}$, while CAM5 estimates a rate of 1.4×10^{20} molecules $\mathrm{s^{-1}}$ $\mathrm{Pa^{-1}}$. At lower altitudes, CAM5 gives a greater rate of ozone loss than CAM4. Both models show a peak in the ozone loss rate around 600 hPa with values of about 0.5×10^{20} molecules $\mathrm{s^{-1}}$ $\mathrm{Pa^{-1}}$ in CAM5, and about 0.4×10^{20} molecules $\mathrm{s^{-1}}$ $\mathrm{Pa^{-1}}$ in CAM4. Overall, as found in Fig. 1 (as confirmed through comparisons with ozonesonde data) and shown in Fig. 5, CAM5 is more efficient in producing ozone than CAM4 in most of the atmosphere.

4.4 Global burdens

Table 1 compares the annual mean tropospheric burden of HO_x, NO_x, gaseous NO_y, and the ratios of $OH : HO_2$ and $NO_x : NO_y$ in both CAM4 and CAM5 for both the control run and aviation NO_x-perturbed run. The comparison of the burdens presented in Table 1 indicates that the background atmosphere is relatively different between the two models (e.g., $\sim$ 8.1 % difference in the background O_3). While such

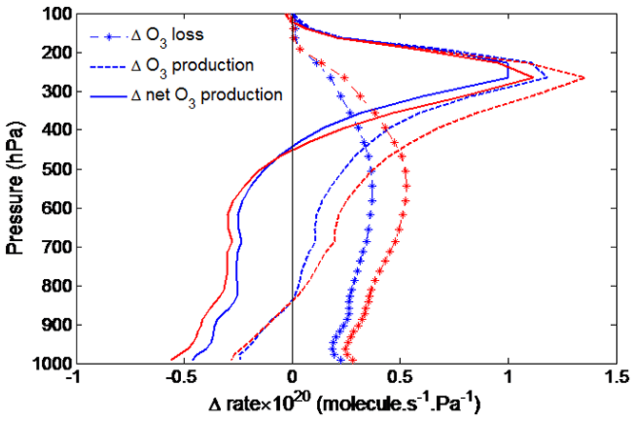

Figure 5. Vertical profile describing the aviation NO_x-induced change in the rate of O_3 production with height (results are shown in red for CAM5 and in blue for CAM4). Net rate of ozone production (solid line), the gross rate of ozone production (dashed line), and the rate of ozone loss (dotted line) are shown. Production and loss rates are calculated as zonal and meridional means.

differences seem to be smaller compared to the intermodel uncertainty (±25 %) reported in Stevenson et al. (2006), there is about a 11.8 % difference in the aviation NO_x-induced annual mean tropospheric O_3 response.

As shown in Table 1, the ratio of $NO_x : NO_y$ is about 7 % higher in the CAM5-perturbed run than in CAM4-perturbed run implying a smaller shift of the $NO_x : NO_y$ relationship to NO_y in CAM5. The smaller shift of the $NO_x : NO_y$ relationship to NO_y in CAM5 is tied to heterogeneous reactions and related to less aerosol surface area density in CAM5 compared to CAM4. Under lower aerosol surface-area density, heterogeneous reaction can be less effective in moving NO_x to NO_y and this results in more OH, and shorter CH_4 lifetime (as seen in Table 2). Heterogonous reactions that are included in CAM chemical mechanism are listed in Reactions (1)–(3).

$$N_2O_5 \rightarrow 2HNO_3 \quad (1)$$

$$NO_3 \rightarrow HNO_3 \quad (2)$$

$$NO_2 \rightarrow 0.5 \times (OH + NO + HNO_3) \quad (3)$$

As such, due to less efficient transfer of NO_x to NO_y in CAM5 compared to CAM4 there is more nitrogen available in its reactive form (NO_x) to trigger the ozone formation reactions in CAM5, resulting in higher aviation NO_x-induced ozone perturbation.

4.5 Ozone

The NO_x-induced changes in tropospheric ozone are complicated by two stages, a short-term increase in O_3 concentrations associated with a positive forcing, and a long-term reduction of O_3 concentrations tied to the aviation-induced methane decrease. The long-term reduction is associated with negative forcing (Wild et al., 2001; Stevenson et al., 2004). The short-term O_3 forcing is one of the major contributors to the overall aviation forcing and dominates the net O_3 forcing (Lee et al., 2009; Holmes et al., 2011). Since our simulations were performed with fixed CH_4 mixing ratios at the boundary layer, the calculated changes in O_3 concentration are the short-term changes.

The aviation NO_x-induced ozone perturbation is shown in Fig. 6. Model results from CAM5 are shown in the top panel while CAM4 is in the bottom. The left column shows the mean zonal ozone perturbation for January, while the right column shows July. As shown in Fig. 6, CAM5 produces a greater amount and wider distribution of ozone in the UTLS region for both months. The pattern and the localized maximum of the ozone perturbation at 200 hPa in the NH are about the same in both CAM4 and CAM5. The tropospheric mean change in O_3 is higher in CAM5 than CAM4 for both January and July. In July, CAM5 generates a tropospheric mean ozone perturbation of 1.16 ppb (compared to 1.0 in CAM4). In January, CAM5 generates a tropospheric mean ozone perturbation of 1.18 ppb (compared to 1.1 in CAM4). Overall, aviation NO_x emissions from the year 2006 yield an annual tropospheric mean O_3 perturbation of 1.2 ppb (2.4%) in CAM5 and 1.0 ppb (1.9 %) in CAM4. The annual mean O_3 perturbation peaks at 8.2 ppb (6.4 %) in CAM5 and 8.8 ppb (5.2 %) in CAM4. Despite the greater production of annual mean O_3 in CAM5, the peak is slightly lower in CAM5 compared to CAM4, since the produced O_3 is more distributed towards the surface in CAM5.

As shown in Fig. 6, the UTLS ozone perturbation is much greater in July than in January for both models. This is due to differences in the length of daylight between those months, increased photochemistry, and higher aviation NO_x emissions in July (as shown in Fig. 4). The increased daylight allows more photolysis of NO_2 to occur, which generates O_3 (Reactions P5 and P6). Also note the differences in ozone perturbations in the lower troposphere between January and July. In the summer, the ozone perturbation at lower altitudes is weaker due to greater surface deposition and also the shorter photochemical lifetime of ozone through increased water vapor (and more HO_x giving increased ozone loss) (Hodnebrog et al., 2011). Additionally, both models show the maximum ozone impact increasing towards high latitudes in the NH in July. A similar result was found by Hoor et al. (2009) who showed a maximum zonal mean ozone perturbation centered around 75° N during June.

As shown in both months and models, a mid-latitudinal perturbation extends from 400 hPa down towards the surface. This feature agrees with past studies by Hoor et al. (2009), Koffi et al. (2010), and Hodnebrog et al. (2011). Hoor et al. (2009) notes that this feature is due to more vigorous boundary layer mixing and convective transport into the free troposphere during the summer.

As shown in Fig. 7, annual mean column ozone changes are relatively zonally well mixed, however, several "hotspots" in both CAM5 and CAM4 exist just north of the

Table 1. Annual tropospheric mean burden of HO_x, NO_x, gaseous NO_y and the ratios of $OH:HO_2$ and $NO_x:NO_y$ in both CAM5 and CAM4 for both the control run (_c) and aviation NO_x-perturbed run (_p).

	O_3 (kg)	OH (kg)	HO_2 (kg)	HO_x (kg)	OH/HO_2	NO_x (kgN)	NO_y (kgN)	$NO_x:NO_y$
CAM4_c	3.71×10^{11}	2.11×10^{5}	2.59×10^{7}	2.61×10^{7}	8.15×10^{-3}	1.20×10^{8}	7.69×10^{8}	0.156
CAM4_p	3.79×10^{11}	2.17×10^{5}	2.58×10^{7}	2.60×10^{7}	8.39×10^{-3}	1.24×10^{8}	7.96×10^{8}	0.156
CAM5_c	3.41×10^{11}	2.68×10^{5}	2.73×10^{7}	2.76×10^{7}	9.82×10^{-3}	1.24×10^{8}	7.30×10^{8}	0.170
CAM5_p	3.50×10^{11}	2.75×10^{5}	2.72×10^{7}	2.75×10^{7}	1.01×10^{-2}	1.29×10^{8}	7.73×10^{8}	0.167

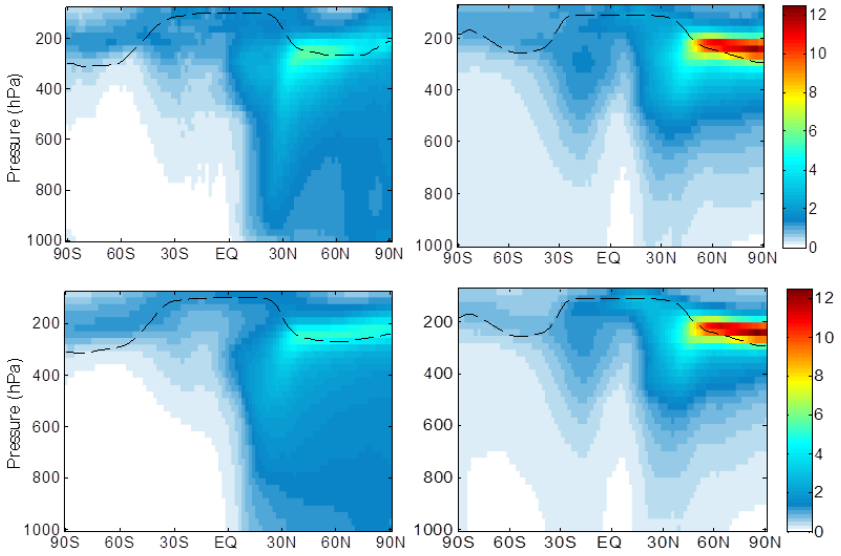

Figure 6. Zonal mean perturbations of ozone (ppb) during January (left) and July (right). CAM5 is in the top panel, while CAM4 is on the bottom. The dashed line indicates the tropopause.

Mediterranean and off the western coast of Europe. A more uniform spread is seen over Europe, the western half of Asia, the Atlantic Ocean, and a small strip at about 45° N in the Pacific Ocean. These "hotspots" are stronger in CAM5 and peak at about 2.3 DU compared to 2.1 DU in CAM4. As expected, the ozone impact is very small in the SH. A sharp ozone gradient exists in the NH subtropics, as was also seen in previous studies. The ozone concentration continues to increase, with the maximum values between 30 and 60° N. Hoor et al. (2009) and Hodnebrog et al. (2011) found a similar distribution. Overall, aviation NO_x emissions from the year 2006 lead to a 1.0 and 0.9 DU change in annual global mean ozone column in CAM5 and CAM4, respectively.

4.6 HO_x

The hydroxyl radical (OH) plays an important role in the creation of atmospheric ozone. It is the primary oxidizing agent of the troposphere, removing greenhouse gases such as CH_4, CO, HCFCs, and others. Production of OH by O_3 is given by Reaction (L2). Figure 8 shows the increase in aviation-induced zonal mean annual OH perturbations.

Similar to ozone, the impact of aviation emitted NO_x on tropospheric OH production is largest in July. This increase in OH during the summer months is also due to the enhanced photochemistry. Aircraft emissions have the largest zonal mean ozone impact in the UTLS region in mid- and high latitudes in the NH between 40 and 90° N. However, the OH perturbation is more concentrated south of the O_3 perturbations. The more southern position of OH is due to the increased humidity and the lower solar zenith angle, which are essential to produce the excited oxygen atom ($O(^1D)$) and hence higher OH concentrations. This result agrees well with recent studies by Hoor et al. (2009) and Hodnebrog et al. (2011). Additionally, there is a greater perturbation of OH extending towards the surface over mid-latitudes than there was of O_3. This is due to the increased production of HO_x in the mid-troposphere triggered by O_3 photolysis and the presence of water vapor. Additionally, both models show OH perturbations extending from 400 hPa down to the surface above 40° N. This feature is much weaker in January because the UV actinic flux necessary for OH production is much smaller in the Northern Hemisphere.

Between the two models, the OH concentration is higher in CAM5 than CAM4. This is a result of higher O_3 production

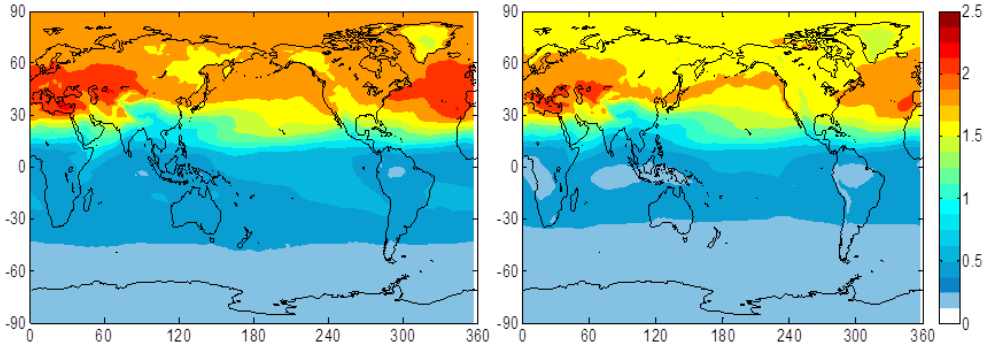

Figure 7. Yearly mean perturbations of the ozone column (ΔDU) based on 2006 aircraft NO_x emissions. CAM5 is on the left, while CAM4 is on the right.

Table 2. Global annual average CH_4 lifetimes against reaction with OH, as calculated by CAM4 and CAM5 for the control run and for the NO_x perturbation run. The relative change between runs is displayed in the right-most column. It is noted that the calculated lifetimes are shorter than the CH_4 lifetime derived based on Methyl chloroform analysis (Prather et al., 2012).

CH_4 lifetime (yr)	Control run	Perturbed run	Rel change (%)
CAM5	7.09	6.97	1.69
CAM4	8.83	8.71	1.40

in CAM5. In July, the CAM5 aviation NO_x-induced tropospheric mean OH perturbation is 1.2×10^4 molecules cm^{-3} (compared to 9.1×10^3 in CAM4). In January, the CAM5 aviation NO_x-induced tropospheric mean OH perturbation is 9.4×10^3 molecules cm^{-3} (compared to 6.4×10^3 in CAM4). Overall, aviation NO_x emissions from the year 2006 lead to an annual tropospheric mean OH perturbation of 1.1×10^4 molecules cm^{-3} in CAM5 and 7.8×10^3 molecules cm^{-3} in CAM4.

Figure 9 shows the CAM4 and CAM5 HO_2 perturbations due to aviation NO_x emissions. Areas that experience an increase in HO_2 concentrations are shown in red and areas that experience a decrease in HO_2 are in blue. Increases in NO_x emissions from aviation increases OH levels by shifting the HO_x balance in favor of OH production, given by Reaction (P4) (Stevenson et al., 2004; Berntsen et al., 2005; Köhler et al., 2008). This process results in HO_2 loss at cruise altitudes. As expected, the areas of HO_2 loss correspond to the areas that experienced an increase in OH concentrations.

In January, there is a greater rate of HO_2 consumption in the UTLS region in CAM5 than there is in CAM4 due to higher OH production. Following Reaction (P4), this HO_2 reacts with aircraft emitted NO to give OH and NO_2. Similarly, the rate of HO_2 consumption is also greater in the UTLS region during July in CAM5 as well. When comparing Fig. 9 with Fig. 8, the locations of maximum HO_2 loss correspond with the locations of maximum OH concentration changes, indicating that Reaction (P4) is a significant reaction in OH production in the UTLS region. At lower altitudes in July, the transported ozone is photolyzed in the presence of water vapor, thus increasing OH, and subsequently HO_2.

4.7 CH_4

The hydroxyl radical OH is the largest sink of CH_4 in the atmosphere. As the OH concentration is effected by aircraft emissions, so is the methane concentration and its lifetime.

Figure 10 shows the aviation-induced annual zonal averaged CH_4 loss rate for CAM5 (left) and CAM4 (right). In both CAM5 and CAM4, the change in methane loss is mostly confined to the NH at a location south of the OH perturbation (between 0 and 30° N). This predominately occurs due to the increase in the methane-OH reaction rate constant with higher temperatures at lower altitudes. As such, in both models the position of the maximum CH_4 loss is below the cruise altitude. As shown in Fig. 10, the CH_4 loss is higher in CAM5 than CAM4 due to the higher production of aviation-induced OH in CAM5. Table 2 shows the reduction in methane lifetimes as calculated for both CAM4 and CAM5.

Table 2 shows the global annual average CH_4 lifetimes against reaction with OH, as calculated by CAM4 and CAM5 for the background (control) run and the NO_x-perturbed run. It is noted that same as most other models (Voulgarakis et al., 2013 and Naik et al., 2013), the calculated lifetimes here are shorter than the CH_4 lifetime derived based on methyl chloroform analysis (Prather et al., 2012). The change in CH_4 lifetime is also presented as the percent change in lifetime. The reduction in CH_4 lifetime calculated in CAM5 and CAM4 is 1.69 % (2.50 % $[TgN\,yr^{-1}]^{-1}$) and 1.40 % (1.71 % $[TgN\,yr^{-1}]^{-1}$), respectively, excluding the feedback of changes in methane concentration on its own lifetime (e.g., Prather, 1994; Fuglestvedt et al., 1999; Wild et al., 2001 and IPCC, 2007). The CAM4 reduction in CH_4 lifetime falls within the -1.4 ± 0.4 (% $[TgN\,yr^{-1}]^{-1}$) to

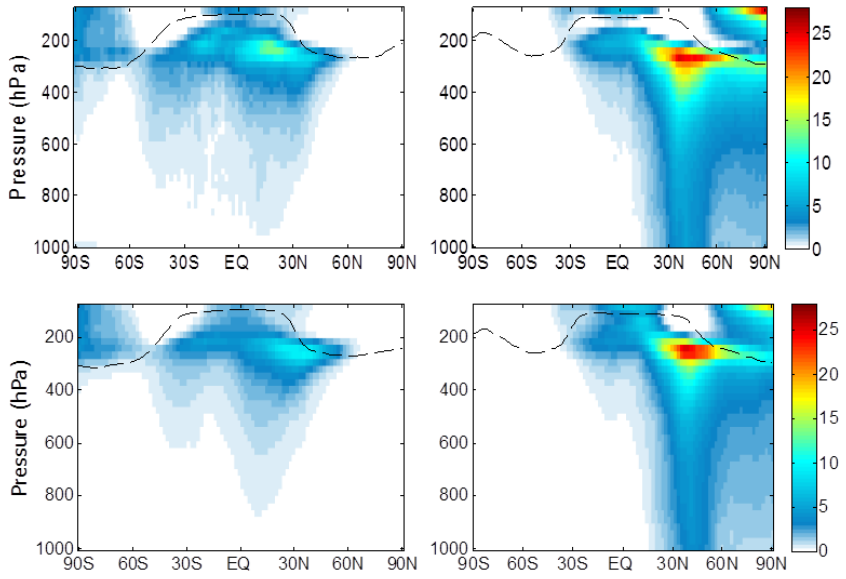

Figure 8. Aviation-induced OH perturbations ($10^{-4}\,\Delta$molec cm^{-3}) during January (left) and July (right). CAM5 is in the top panel, while CAM4 is in the bottom. The dashed line indicates the tropopause.

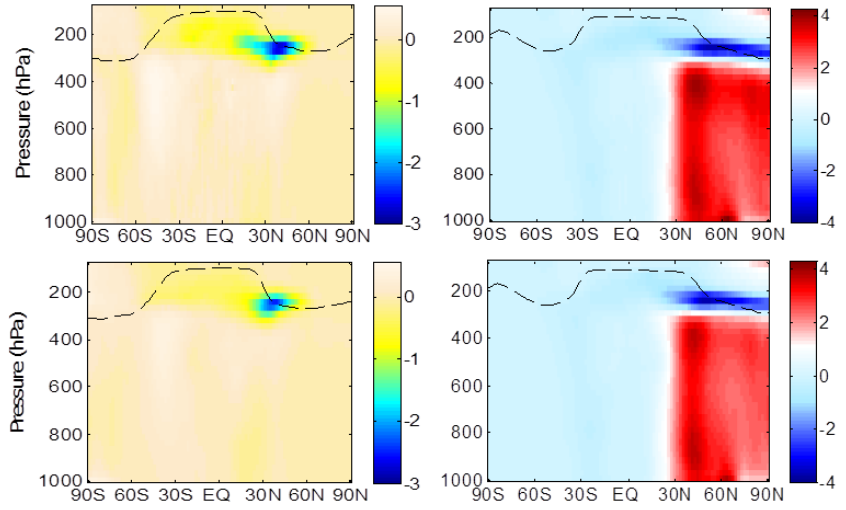

Figure 9. As in Fig. 7, but for HO_2 ($10^{-6}\,\Delta$molec cm^{-3}).

-1.6 ± 0.37 (% [TgN yr^{-1}]$^{-1}$) range reported by Hodnebrog et al. (2011). The CAM5 simulated change in CH_4 lifetime is greater than the upper range reported by Hodnebrog et al. (2011). Inclusion of the aviation-induced methane feedback on its lifetime further decreases the lifetime by a factor of 1.4 (IPCC, 2001). The greater reduction of the CH_4 lifetime in CAM5 is the result of a greater increase in the aviation-induced OH concentration in CAM5.

4.8 Aviation NO_x-induced ozone radiative forcings

The aviation NO_x-induced short-term O_3 RFs were calculated as the difference of the radiation imbalance between the NO_x-perturbed and control simulations at the tropopause calculated with the UIUC RTM, excluding the effects of stratospheric adjustment. Figure 11 shows the yearly averaged short-term ozone RF for CAM5 (left) and CAM4 (right). Both models show the greatest RF in the NH between 30 and 60° N with highest RF changes over southern Europe and the Middle East. As expected, the O_3 RF from aviation is low in the SH. The greatest RF values in the SH are over the SH tropical Pacific Ocean and are most likely due to air traffic between Australia and the United States. Interestingly, radiative forcing values over Asia are relatively low, given the amount of NO_x emissions from this area. Additionally, it appears that the maximum radiative forcing from Europe's

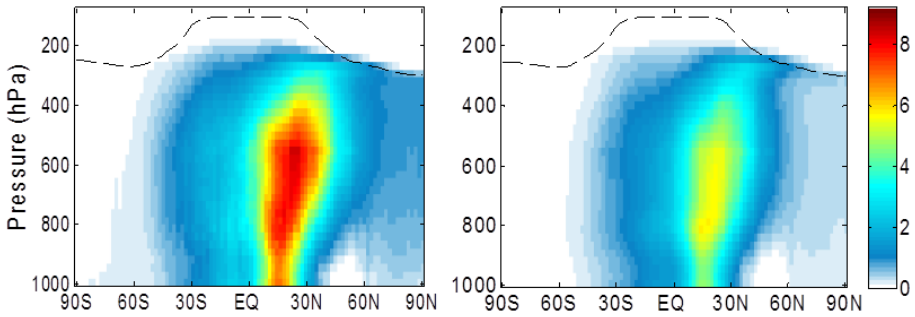

Figure 10. Annual zonal averaged CH_4 loss (10^{-3} Δmolec cm^{-3} s) induced by aviation NO_x emissions. CAM5 is on the left, CAM4 is on the right. The dashed line indicates the tropopause.

emissions has shifted to the Mediterranean, indicating that these aircraft emissions have a maximum impact downwind of the source. These results agree well with Hodnebrog et al. (2011).

The associated global mean short-term ozone RF is 40.3 and 36.5 mWm^{-2} in CAM5 and CAM4, respectively. CAM5 has a greater annual ozone RF, due to the greater ozone perturbation, which largely accounts for the differences in radiative forcings. It is noted that Fuglestvedt et al. (2008) compares the aviation contribution in changing the radiative forcing to the contribution from other transportation sectors.

5 Conclusions

Aviation NO_x-induced effects on ozone and the oxidative capacity were evaluated using two different atmospheric components of CESM, namely, CAM4 and CAM5. This study is the first evaluation of aviation NO_x effects in CAM5 which simulates the size distribution of aerosols, both internal and external mixing of aerosols, and chemical and optical properties of aerosols. The differences between the aviation NO_x-induced effects presented here are mainly caused by the different treatments of aerosols between the two models.

CAM5 and CAM4 simulate background ozone to within 13 and 18 % (on average and at all the locations), respectively, compared to ozonesonde data sets. Based on the comparison with ozonesonde observations, CAM5 was more accurate at determining the ozone distribution in the troposphere–lower stratosphere.

Aviation-induced O_3 is higher in CAM5 than CAM4 with an annual tropospheric mean O_3 perturbation of 1.2 ppb (2.4 %) in CAM5 and 1.0 ppb (1.9 %) in CAM4. In July, CAM5 generates an aviation NO_x-induced tropospheric mean ozone perturbation of 1.16 ppb (compared to 1.0 in CAM4) with a corresponding value of 1.18 ppb in January (compared to 1.1 in CAM4).

As found in previous studies, the maximum effect from aircraft NO_x emissions on ozone is in the NH upper troposphere–lower stratosphere region. This is due to the high frequency of subsonic aircraft flying in this region. The aircraft-induced ozone perturbation is greater in the NH summer due to the enhanced photochemistry. In January, the ozone perturbation mixes more towards the surface due to the longer photochemical lifetime of ozone and the slower surface deposition rate than in July.

The hydroxyl perturbations are located to the south and at a lower altitude than the position of the maximum change in ozone. This is due to the lower zenith angle and increased humidity which are essential to produce the excited oxygen atom ($O(^1D)$) and hence higher OH concentrations. Overall, the aviation NO_x-induced change in OH is higher in CAM5 in accordance with higher ozone production. The induced changes in OH concentrations increase the methane (CH_4) loss rate and reduce its lifetime by 1.69 and 1.40 % in CAM5 and CAM4, respectively.

Results indicate a global mean O_3 RF of 40.3 and 36.5 mWm^{-2} in CAM5 and CAM4, respectively. Both models agree that the maximum O_3 radiative forcing is between 30 and 60° N. However, it is interesting to note that it appears that the maximum RF is downwind of a local maximum NO_x source.

It is noted that while the simulated change in ozone is relatively different between the two models, the difference between CAM4 and CAM5 ozone responses is considerably smaller than the current estimates of the uncertainty in aviation effects on ozone. The difference in aviation NO_x-induced effects between the two models is related to the difference between the two models configuration used in this study (i.e., difference in aerosols treatment). More detailed analyses are required to explore the impact of the differences in the representation of the background atmosphere and treatment of aerosols processes on aviation NO_x-induced effects to a greater extent.

Acknowledgements. The authors would like to thank the Federal Aviation Administration, Aviation Climate Change Research Initiative (ACCRI) for support under contract no. 10-C-NE-UI amendment 001 and The Partnership for AiR Transportation Noise and Emissions Reduction (PARTNER). The opinions, findings, and conclusions or recommendations expressed in this material

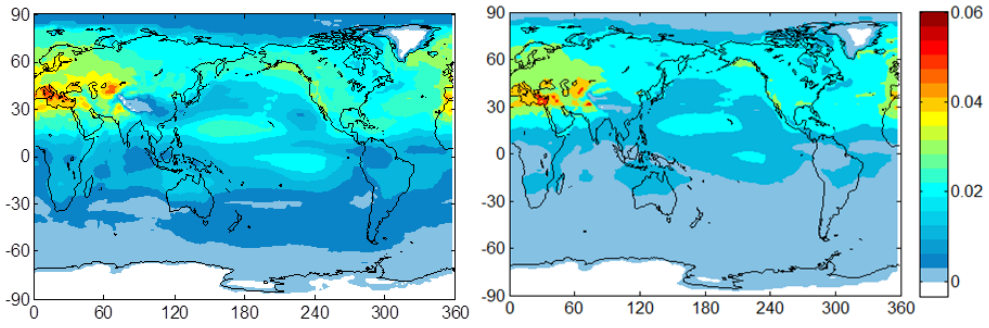

Figure 11. Yearly mean radiative forcing (mWm^{-2}) from O_3 due to aviation NO_x emissions. CAM5 is on the left, CAM4 is on the right.

are those of the authors and do not necessarily reflect the views of ACCRI, PARTNER, or the FAA. This work was partially supported by the US Department of Transportation, the Illinois Department of Transportation and the Transportation Research and Analysis Computing Center. The authors would like to thank the National Center for Atmospheric Research (NCAR) for the support with computing time and NCAR is supported by the National Science Foundation (NSF). The CESM project (which includes CAM4, CAM5 and CAM-chem) is supported by the National Science Foundation and the Office of Science (BER) of the US Department of Energy. The authors would like to also thank F. Vitt (NCAR) for his help in integrating aviation NO_x emissions into CAM5.

Edited by: J. West

References

Berntsen, T. K., Fuglestvedt, J. S., Joshi, M. M., Shine, K. P., Stuber, N., Ponater, M., Sausen, R., Hauglustaine, D. A., and Li, L.: Response of climate to regional emissions of ozone precursors: Sensitivities and warming potentials, Tellus B, 57, 283–304, 2005.

Brasseur, P. G., Weber, B., Damoah, R., Douglass, A. R., Jacobson, M. Z., Lee, H., Liang, Q., Olsen, S. C., Oman, L. D., Ott, L., Pawson, S., Selkirk, H., Sokolov, A., Stolarski, R. S., Unger, N., and Wuebbles, D. J.: Model intercomparison of ozone sensitivity to NO_x emissions in the vicinity of the extratropical tropopause, Geophys. Res. Lett., submitted, 2014.

Conley, A. J., Lamarque, J.-F., Vitt, F., Collins, W. D., and Kiehl, J.: PORT, a CESM tool for the diagnosis of radiative forcing, Geosci. Model Dev., 6, 469–476, doi:10.5194/gmd-6-469-2013, 2013.

Derwent, R., Friedl, R., Karol, I. L., Kirchhoff, V. W. J. H., Ogawa, T., Rossi, M. J., and Wennberg, P.: Impacts of aircraft emissions on atmospheric ozone, edited by: Penner, J. E., Lister, D. H., Griggs, D. J., Dokken, D. J., and McFarland, M.: Aviation and the global atmosphere. A special report of IPCC working groups I and III, Cambridge Unviersity Press, Cambridge, UK, 27–64, 1999.

Derwent, R. G., Collins, W. J., Johnson, C. E., and Stevenson, D. S.: Transient behavior of tropospheric ozone precursors in a global 3-D CTM and their indirect greenhouse effects, Clim. Change, 49, 463–487, 2001.

Emmons, L. K., Walters, S., Hess, P. G., Lamarque, J.-F., Pfister, G. G., Fillmore, D., Granier, C., Guenther, A., Kinnison, D., Laepple, T., Orlando, J., Tie, X., Tyndall, G., Wiedinmyer, C., Baughcum, S. L., and Kloster, S.: Description and evaluation of the Model for Ozone and Related chemical Tracers, version 4 (MOZART-4), Geosci. Model Dev., 3, 43–67, doi:10.5194/gmd-3-43-2010, 2010.

Fuglestvedt, J. S., Berntsen, T., Isaksen, I. S. A., Huiting, M., Liang, X.-Z., and Wang, W.-C.: Climatic forcing of nitrogen oxides through changes in tropospheric ozone and methane; global 3D model studies, Atmos. Environ., 33, 961–977, 1999.

Fuglestvedt, J. S., Berntsen, T., Myhre, G., Rypdal, K., and Skeie, R. B.: Climate forcing from the Transport Sectors, P. Natl. Acad. Sci. USA, 105, 454–458, 2008.

Gent, P. R., Danabasoglu, G., Donner, L. J., Holland, M. M., Hunke, E. C., Jayne, S. R., Lawrence, D. M., Neale, R. B., Rasch, P. J., Vertenstein, M., Worley, P. H., Yang, Z.-L., and Zhang, M.: The community climate system model version 4, J. Climate, 24, 4973–4991, 2011.

Gettelman, A., Morrison, H., and Ghan, S. J.: A new two-moment bulk stratiform cloud microphysics scheme in the NCAR Community Atmosphere Model (CAM3), Part II: Single-column and global results, J. Climate, 21, 3660–3679, 2008.

Gettelman, A., Liu, X., Ghan, S. J., Morrison, H., Park, S., Conley, A. J., Klein, S. A., Boyle, J., Mitchell, D. L., and Li, J.-L. F.: Global simulations of ice nucleation and ice supersaturation with an improved cloud scheme in the Community Atmosphere Model, J. Geophys. Res., 115, D18216, doi:10.1029/2009JD013797, 2010.

Gettelman, A., Liu, X., Barahona, D., Lohmann, U., and Chen, C.: Climate impacts of ice nucleation, J. Geophys. Res., 117, D20201, doi:10.1029/2012JD017950, 2012.

Gettelman, A., Morrison, H., Terai, C. R., and Wood, R.: Microphysical process rates and global aerosol-cloud interactions, Atmos. Chem. Phys., 13, 9855–9867, doi:10.5194/acp-13-9855-2013, 2013.

Hodnebrog, Ø., Berntsen, T. K., Dessens, O., Gauss, M., Grewe, V., Isaksen, I. S. A., Koffi, B., Myhre, G., Olivié, D., Prather, M. J., Pyle, J. A., Stordal, F., Szopa, S., Tang, Q., van Velthoven, P., Williams, J. E., and Ødemark, K.: Future impact of non-land based traffic emissions on atmospheric ozone and OH – an optimistic scenario and a possible mitigation strategy, Atmos. Chem. Phys., 11, 11293–11317, doi:10.5194/acp-11-11293-2011, 2011.

Holmes, C. D., Tang, Q., and Prather, M. J.: Uncertainties in climate assessment for the case of aviation NO, P. Natl. Acad. Sci. USA, 108, 10997–11002, 2011.

Hoor, P., Borken-Kleefeld, J., Caro, D., Dessens, O., Endresen, O., Gauss, M., Grewe, V., Hauglustaine, D., Isaksen, I. S. A., Jöckel, P., Lelieveld, J., Myhre, G., Meijer, E., Olivie, D., Prather, M., Schnadt Poberaj, C., Shine, K. P., Staehelin, J., Tang, Q., van Aardenne, J., van Velthoven, P., and Sausen, R.: The impact of traffic emissions on atmospheric ozone and OH: results from QUANTIFY, Atmos. Chem. Phys., 9, 3113–3136, doi:10.5194/acp-9-3113-2009, 2009.

IPCC: Aviation and the global atmosphere, Intergovernmental Panel on Climate Change, edited by: Penner, J. E., Lister, D. H., Griggs, D. J., Dokken, D. J., and McFarland, M., Cambridge University Press, Cambridge, UK, 1999.

IPCC: Climate change, The scientific basis. Contribution of Working Group I to the Third Assessment Report of the Intergovernmental Panel on Climate Change, Houghton, J. T., Ding, Y., Griggs, D. J., Noguer, M., van der Linden, P. J., Dai, X., Maskell, K., and Johnson, C. A., Cambridge University Press, Cambridge, UK, 2001.

IPCC: Climate change, The physical science basis. Contribution of Working Group I to the Fourth Assessment Report of the Intergovernmental Panel on Climate Change, edited by: Solomon, S., Qin, D., Manning, M., Marquis, M., Averyt, K., Tignor, M. M. B., Miller, H. L., and Chen, Z., Cambridge University Press, Cambridge, UK, 2007.

Jain, A. K., Briegleb, B. P., Minschwaner, K., and Wuebbles, D. J.: Radiative forcings and global warming potentials of 39 greenhouse gases, J. Geophys. Res., 105, 20773–20790, doi:10.1029/2000JD900241, 2000

Koffi, B., Szopa, S., Cozic, A., Hauglustaine, D., and van Velthoven, P.: Present and future impact of aircraft, road traffic and shipping emissions on global tropospheric ozone, Atmos. Chem. Phys., 10, 11681–11705, doi:10.5194/acp-10-11681-2010, 2010.

Köhler, M. O., Radel, G., Dessens, O., Shine, K. P., Rogers, H. L., Wild, O., and Pyle, J. A.: Impact of perturbations to nitrogen oxide emissions from global aviation, J. Geophys. Res., 113, D11305, doi:10.1029/2007JD009140, 2008.

Lamarque, J.-F., Emmons, L. K., Hess, P. G., Kinnison, D. E., Tilmes, S., Vitt, F., Heald, C. L., Holland, E. A., Lauritzen, P. H., Neu, J., Orlando, J. J., Rasch, P. J., and Tyndall, G. K.: CAM-chem: description and evaluation of interactive atmospheric chemistry in the Community Earth System Model, Geosci. Model Dev., 5, 369–411, doi:10.5194/gmd-5-369-2012, 2012.

Lee, D. S., Fahey, D. W., Forster, P. M., Newton, P. J., Wit, R. C. N., Lim, L. L., Owen, B., and Sausen, R.: Aviation and global climate change in the 21st century, Atmos. Environ., 43, 3520–3537, 2009.

Medeiros, B., Williamson, D. L., Hannay, C., and Olson, J. G.: Southeast Pacific stratocumulus in the Community Atmosphere Model, J. Climate, 25, 6175–6192, 2012.

Morrison, H. and Gettelman, A.: A new two-moment bulk stratiform cloud microphysics scheme in the NCAR Community Atmosphere Model (CAM3), Part I: Description and numerical tests, J. Climate, 21, 3642–3659, 2008.

Naik, V., Jain, A. K., Patten, K. O., and Wuebbles, D. J.: Consistent sets of atmospheric lifetimes and radiative forcings on climate for CFC replacements: HCFCs and HFCs, J. Geophys. Res., 105, 6903–6914, doi:10.1029/1999JD901128, 2000.

Naik, V., Voulgarakis, A., Fiore, A. M., Horowitz, L. W., Lamarque, J.-F., Lin, M., Prather, M. J., Young, P. J., Bergmann, D., Cameron-Smith, P. J., Cionni, I., Collins, W. J., Dalsøren, S. B., Doherty, R., Eyring, V., Faluvegi, G., Folberth, G. A., Josse, B., Lee, Y. H., MacKenzie, I. A., Nagashima, T., van Noije, T. P. C., Plummer, D. A., Righi, M., Rumbold, S. T., Skeie, R., Shindell, D. T., Stevenson, D. S., Strode, S., Sudo, K., Szopa, S., and Zeng, G.: Preindustrial to present-day changes in tropospheric hydroxyl radical and methane lifetime from the Atmospheric Chemistry and Climate Model Intercomparison Project (ACCMIP), Atmos. Chem. Phys., 13, 5277–5298, doi:10.5194/acp-13-5277-2013, 2013.

Neale, R. B., Richter, J., Park, S., Lauritzen, P. H., Vavrus, S. J., Rasch, P. J., and Zhang, M.: The mean climate of the Community Atmosphere Model (CAM4) in forced SST and fully coupled experiments, J. Climate, 26, 5150–5168, doi:10.1175/JCLI-D-12-00236.1, 2013.

Olsen, S. C., Wuebbles, D. J., and Owen, B.: Comparison of global 3-D aviation emissions datasets, Atmos. Chem. Phys., 13, 429–441, doi:10.5194/acp-13-429-2013, 2013a.

Olsen, S. C., Brasseur, G. P., Wuebbles, D. J., Barrett, S., Dang, H., Eastham, S. D., Jacobson, M. Z., Khodayari, A., Selkirk, H., Sokolov, A., and Unger, N.: Comparison of model estimates of the effects of aviation emissions on atmospheric ozone and methane, Geophys. Res. Lett., 40, 6004–6009, doi:10.1002/2013GL057660, 2013b.

Patten, K. O., Khamaganov, V. G., Orkin, V. L., Baughcum, S. L., and Wuebbles, D. J.: OH reaction rate constant, IR absorption spectrum, ozone depletion potentials and global warming potentials of 2-bromo-3,3,3-trifluoropropene, J. Geophys. Res., 116, D24307, doi:10.1029/2011JD016518, 2011.

Prather, M. J.: Lifetimes and eigenstates in atmospheric chemistry, Geophys. Res. Lett., 21, 801–804, 1994.

Prather, M. J., Holmes, C. D., and Hsu, J.: Reactive greenhouse gas scenarios: Systematic exploration of uncertainties and the role of atmospheric chemistry, Geophys. Res. Lett., 39, doi:10.1029/2012GL051440, 2012.

Rienecker, M. M., Suarez, M. J., Todling, R., Bacmeister, J., Takacs, L., Liu, H.-C., Gu, W., Sienkiewicz, M., Koster, R. D., Gelaro, R., Stajner, I., and Nielsen, E.: The GEOS-5 Data Assimilation System-Documentation of versions 5.0.1, 5.1.0, and 5.2.0.NASA/TM-2008-104606, Vol. 27, Technical Report Series on Global Modeling and Data Assimilation, 118 pp., available at: http://gmao.gsfc.nasa.gov/systems/geos5/ (last access: 11 July 2011), 2008.

Rothman, L. S., Jacquemart, D., Barbe, A., Chris Benner, D., Birk, M., Brown, L. R., Carleer, M. R., Chackerian Jr., C., Chance, K., Coudert, L. H., Dana, V., Devi, V. M., Flaud, J.-M., Gamache, R. R., Goldman, A., Hartmann, J.-M., Jucks, K. W., Maki, A. G., Mandin, J.-Y., Massie, S. T., Orphal, J., Perrin, A., Rinsland, C. P., Smith, M. A. H., Tennyson, J., Tolchenov, R. N., Toth, R. A., Vander Auwera, J., Varanasi, P., and Wagner, G.: The HITRAN 2004 molecular spectroscopic database, J. Quant. Spectrosc. Ra., 96, 139–204, doi:10.1016/j.jqsrt.2004.10.008, 2005.

Shine, K. P., Berntsen, T. K., Fuglestvedt, J. S., and Sausen, R.: Scientific issues in the design of metrics for inclusion of oxides of

nitrogen in global climate agreements, P. Natl Acad. Sci. USA., 102, 15768–15773, doi:10.1073/pnas.0506865102, 2005a.

Sillman, S.: Overview: Tropospheric ozone, smog and ozone-NO_x-VOC sensitivity, online, University of Michigan, available at: http://www-personal.umich.edu/~sillman/Sillman-webOZONE.pdf, last access: 11 April 2012.

Stevenson, D. S. and Derwent, R. G.: Does the location of aircraft nitrogen oxide emissions affect their climate impact?, Geophys. Res. Lett., 36, L17810, doi:10.1029/2009GL039422, 2009.

Stevenson, D. S., Doherty, R. M., Sanderson, M. G., Collins, W. J., Johnson, C. E., and Derwent, R. G.: Radiative forcing from aircraft NO_x emissions: Mechanisms and seasonal dependence, J. Geophys. Res., 109, doi:10.1029/2004JD004759, 2004.

Stevenson, D. S., Dentener, F. J., Schultz, M. G., Ellingsen, K., van Noije, T. P. C., Wild, O., Zeng, G., Amann, M., Atherton, C. S., Bell, N., Bergmann, D. J., Bey, I., Butler, T., Cofala, J., Collins, W. J., Derwent, R. G., Doherty, R. M., Drevet, J., Eskes, H. J., Fiore, A. M., Gauss, M., Hauglustaine, D. A., Horowitz, L. W., Isaksen, I. S. A., Krol, M. C., Lamarque, J.-F., Lawrence, M. G., Montanaro, V., Müller, J.-F., Pitari, G., Prather, M. J., Pyle, J. A., Rast, S., Rodriguez, J. M., Sanderson, M. G., Savage, N. H., Shindell, D. T., Strahan, S. E., Sudo, K., and Szopa, S.: Multi-model ensemble simulations of present-day and near future tropospheric ozone, J. Geophys. Res., 111, D08301, doi:10.1029/2005JD006338, 2006.

Tilmes, S., Lamarque, J.-F., Emmons, L. K., Conley, A., Schultz, M. G., Saunois, M., Thouret, V., Thompson, A. M., Oltmans, S. J., Johnson, B., and Tarasick, D.: Technical Note: Ozonesonde climatology between 1995 and 2011: description, evaluation and applications, Atmos. Chem. Phys., 12, 7475–7497, doi:10.5194/acp-12-7475-2012, 2012.

Tilmes, S., Lamarque, J.-F., Emmons, L. K., Kinnison, D. E., Bardee, C., Deeter, M., and Vitt, F.: Representation of chemistry in CAM4 and CAM5 in the Community Earth System Model (CESM1.2), in preparation, 2014.

Van Vuuren, D. P., Edmonds, J., Kainuma, M., Riahi, K., Thomson, A., Hibbard, K., Hurtt, G. C., Kram, T., Krey, V., Lamarque, J.-F., Masui, T., Meinshausen, M., Nakicenovic, N., Smith, S. J., and Rose, S. K.: The representative concentration pathways: an overview, Clim. Change, 109, 5–31, doi:10.1007/s10584-011-0148-z, 2011.

Voulgarakis, A., Naik, V., Lamarque, J.-F., Shindell, D. T., Young, P. J., Prather, M. J., Wild, O., Field, R. D., Bergmann, D., Cameron-Smith, P., Cionni, I., Collins, W. J., Dalsøren, S. B., Doherty, R. M., Eyring, V., Faluvegi, G., Folberth, G. A., Horowitz, L. W., Josse, B., MacKenzie, I. A., Nagashima, T., Plummer, D. A., Righi, M., Rumbold, S. T., Stevenson, D. S., Strode, S. A., Sudo, K., Szopa, S., and Zeng, G.: Analysis of present day and future OH and methane lifetime in the ACCMIP simulations, Atmos. Chem. Phys., 13, 2563–2587, doi:10.5194/acp-13-2563-2013, 2013.

Weber, M., Dikty, S., Burrows, J. P., Garny, H., Dameris, M., Kubin, A., Abalichin, J., and Langematz, U.: The Brewer-Dobson circulation and total ozone from seasonal to decadal time scales, Atmos. Chem. Phys., 11, 11221–11235, doi:10.5194/acp-11-11221-2011, 2011.

Wild, O., Prather, M. J., and Akimoto, H.: Indirect long-term global cooling from NO_x emissions, Geophys. Res. Lett., 28, 1719–1722, 2001.

Wild, O., Fiore, A. M., Shindell, D. T., Doherty, R. M., Collins, W. J., Dentener, F. J., Schultz, M. G., Gong, S., MacKenzie, I. A., Zeng, G., Hess, P., Duncan, B. N., Bergmann, D. J., Szopa, S., Jonson, J. E., Keating, T. J., and Zuber, A.: Modelling future changes in surface ozone: a parameterized approach, Atmos. Chem. Phys., 12, 2037–2054, doi:10.5194/acp-12-2037-2012, 2012.

Wilkerson, J. T., Jacobson, M. Z., Malwitz, A., Balasubramanian, S., Wayson, R., Fleming, G., Naiman, A. D., and Lele, S. K.: Analysis of emission data from global commercial aviation: 2004 and 2006, Atmos. Chem. Phys., 10, 6391–6408, doi:10.5194/acp-10-6391-2010, 2010.

Youn, D., Patten, K. O., Lin, J.-T., and Wuebbles, D. J.: Explicit calculation of indirect global warming potentials for halons using atmospheric models, Atmos. Chem. Phys., 9, 8719–8733, doi:10.5194/acp-9-8719-2009, 2009.